ADVANCED MATERIALS
www.advmat.de

Multistable Shape-Reconfigurable Architected Materials

*Babak Haghpanah, Ladan Salari-Sharif, Peyman Pourrajab, Jonathan Hopkins, and Lorenzo Valdevit**

Shape-reconfigurable materials (SRMs) are capable of achieving significant morphological change upon application of relatively small loads and maintaining the desired shape when the loading is removed. This deformation is reversible and the original shape is recoverable by reversing the load direction. This property of matter could pave the way for manufacturing of highly adaptable components that are fully reconfigurable based on functionality. For example, a multistable reconfigurable material can be compressed significantly to be transported with considerably less cost before deployment;[1,2] or it can be used to fabricate tools with multiple stable shapes for different purposes. Other foreseeable applications include energy and impact absorption,[3] tunable phononic response,[4] vibration isolation,[5] and programmable metamaterials.[6] Several strategies toward this goal have already been proposed, including foldable origami,[7,8] tension controlled tensegrity structures,[9,10] shape memory morphing materials and structures,[11,12] shape-shifting jamming materials,[13] and modular self-assembled structures.[14–16] In most of these material systems, the ability of the material to morph is very limited in terms of the allowable directions and/or the amplitude of deformation. For instance, origami folding is often based on a single degree-of-freedom rigid folding mechanism and is an energetically inefficient strategy for multiaxial straining. In recent years, a number of studies have introduced materials that are capable of achieving stable geometrical change using the concept of bi-stable negative stiffness elements.[3,17–19] These designs generally require elastomeric constituents with very large yielding or fracture strain in order to achieve the required reconfigurable behavior without material failure: this results in shape-reconfigurable materials with fairly low strength and limited energy absorption capabilities.

Here, we present an analytical model for the behavior of bi-stable structural elements, which provides valuable insights on the mechanical response (including failure) of shape-reconfigurable materials. This model is used to explore a wide multi-parameter design space. We demonstrate a shape-reconfigurable material that is orders of magnitude stronger than previously published concepts, and can be realized in virtually any constituent (polymer, metal, ceramic, or composite). The proposed concepts allow independent multi-axial deformation with high volumetric and morphological change in 2D and 3D lattice materials, based on multistable structural unit cells encompassing living hinges. Each unit cell comprises several bi-stable triangular frames shown in **Figure 1**A (far left) in closed and open configurations. Each triangular subunit consists of a relatively thick base, that resists stretching or bending, and two inclined hinged beams (living hinges) of equal length with angle α from the horizontal line in the open configuration. When a downward vertical force is applied on the top of the triangle in the open configuration, the two inclined beams are pressed against each other, and at a critical force the triangular frame snaps through and collapses into the second stable position (closed), with the oblique beams now making an angle close to $-\alpha$ with respect to the horizontal line. This concept is used to obtain an effective bi-stable hinge mechanism with the angular motion range of 2α, by extending the base and one of the oblique beams, see Figure 1A (middle left). By arranging more triangles in series, multistable hinges with wider range of angular deformation can be obtained, as shown in this figure. The proposed multistable hinge now can be used as a structural building block to design different multi-degree-of-freedom multistable mechanisms with the desired energy and deformation landscape. For instance, four hinge mechanisms can be assembled in a diamond configuration to obtain a planar linear extension unit with significant axial deformation range, as shown in Figure 1A (middle right). Besides axial extension, the presented linear extension unit has two additional kinematic degrees of freedom (i.e., lateral movement and rotation). By using a 3D unit cell, consisting of two planar designs joining each other in two perpendicular planes, the two additional degrees of freedom are suppressed and a unit cell is obtained which can only stretch axially, see Figure 1A (middle right). The introduced morphing mechanisms can be used as design tools to create a wide range of multistable structures in 2D and 3D, for instance, the planar periodic structure shown on Figure 1A (far right), obtained by Cartesian tiling of the previously introduced planar linear extension units. This topology shows a wide range of stable deformed configurations (e.g., O-shaped (i), V-shaped (ii), X-shaped (iii)), see Figure 1B. A quasi-static uniaxial compression test was performed on a 2D linear extension unit with stretch ratio of $\lambda = 1.75$ using a servo electrical INSTRON frame. The structure was attached to the grips in its fully closed position (marked by 1 in inset of Figure 1C) and pulled along the *Y*-direction under displacement control until fully expended (marked by 6 in inset of Figure 1C), after which it was unloaded to the original position. The above procedure was repeated for seven cycles (only three of which are shown in the figure for clarity) and the

Dr. B. Haghpanah, L. Salari-Sharif, P. Pourrajab, Prof. L. Valdevit
Department of Mechanical and Aerospace Engineering
University of California
Irvine, CA, USA 92697
E-mail: valdevit@uci.edu
Prof. J. Hopkins
Department of Mechanical and Aerospace Engineering
University of California
Los Angeles, CA, USA 90095

DOI: 10.1002/adma.201601650

ADVANCED MATERIALS
www.advmat.de

Materials Views
www.MaterialsViews.com

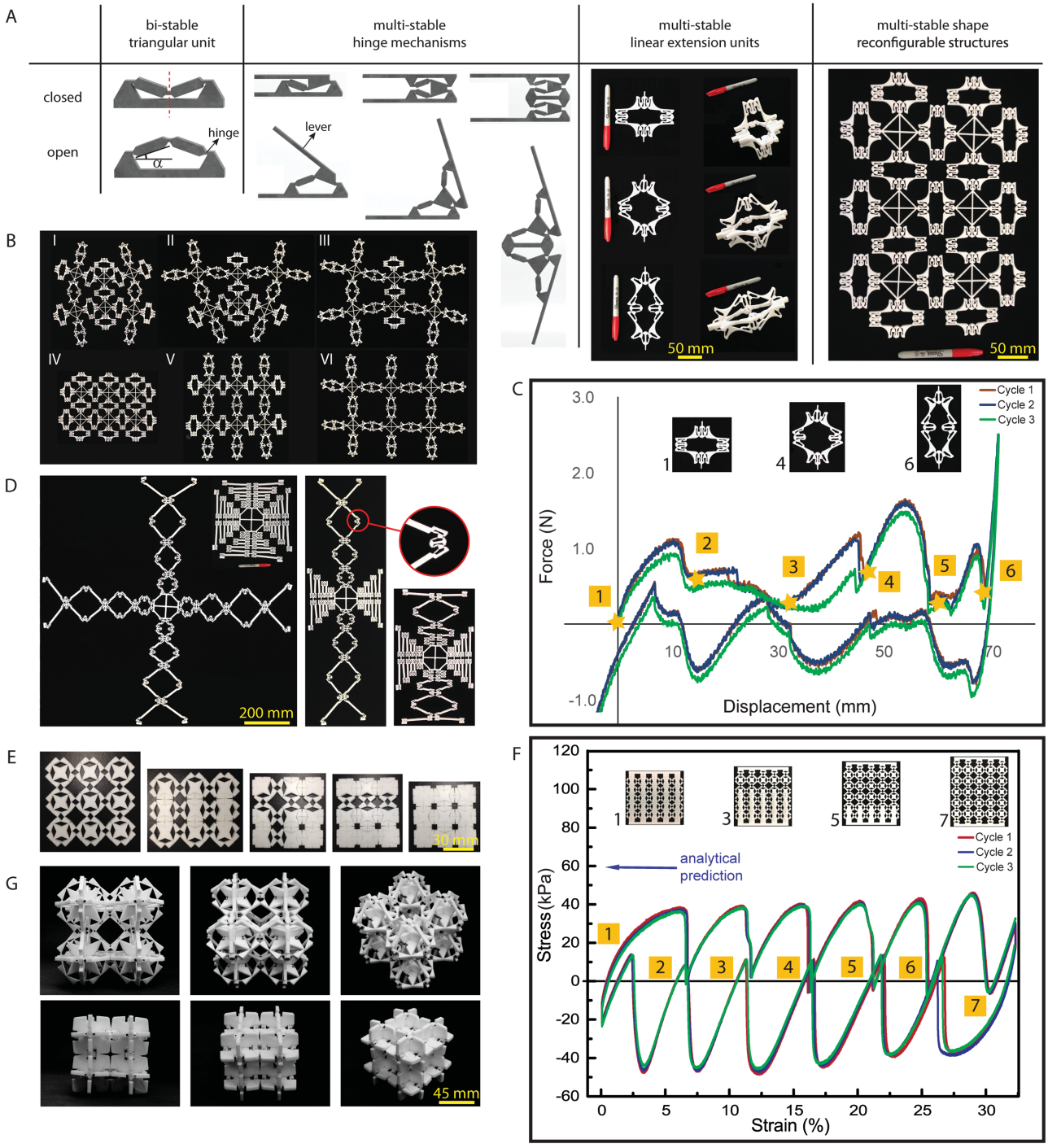

Figure 1. A) A design sequence showing from left to right: a bi-stable triangular unit, effective multistable hinge mechanisms with various range of angular motion, 2D and 3D multistable linear extension units, and a sample periodic shape-reconfigurable structure. B) Different deformed configurations for the shape-reconfigurable planar structure in 1A with stretch ratio of $\lambda = 1.6$, including (i) O-shaped, (ii) V-shaped, (iii) X-shaped, (iv) fully contracted, (v) I-shaped, and (vi) fully expanded. C) Force–displacement response of a linear extension unit with stretch ratio of $\lambda = 1.75$ under quasi-static cyclic loading. D) A highly expandable unit cell with stretch ratio of $\lambda = 3.5$ shown at different deformed configurations. E) A high-strength 2D SRM design at different contracted configurations. F) Force–displacement response of a 5×5 specimen based on the design in (E). G) Prototype of a high-strength 3D SRM with axial contraction ratio of $\lambda = 1.4$. All presented structures are fabricated through laser cutting of sheets of polytetrafluoroethylene (Teflon).

force–displacement response was captured. The results are depicted in Figure 1C (see Section A, Supporting Information). This architecture displays some unique mechanical characteristics: (i) There is a wide range of stretch ($\Delta\lambda = 0.75$)for which the applied load is almost constant (≈1 N). At an extension of ≈70 mm, the full extension is reached and the force

increases dramatically thereafter. (ii) The load–displacement response is non-reversible upon unloading, as will be explained later, resulting in significant cyclic energy dissipation (≈ 70 N.mm). (iii) There are multiple stability points between the minimum and maximum expanded configurations, labeled from 1 to 6, at each of which a further removal of the applied load will result in a stable position (i.e., zero load and positive load–displacement slope). When higher values of stretch ratio are desirable, the unit cell can be designed to include longer levers. The highly expandable unit cell shown in Figure 1D with stretch ratio of $\lambda = 3.5$ is comprised of multiple diamonds in series with each other with the sides of the diamonds gradually decreasing from the side of the unit cell to the center. The general objective in the mechanisms discussed above was to obtain significant amount of deformation at relatively small applied loads. However, in applications such as energy absorption or when the shape-reconfigurable structure is load-bearing, higher values of strength are desirable. The SRM introduced in Figure 1E shows a high-strength design, which is comprised of Cartesian tiling of four old, axisymmetric arrangements of bi-stable triangular units encompassing no levers. The force–displacement cyclic response (seven cycles, only three of which are shown in the figure for clarity) of a 5×5 specimen with stretch ratio of $\lambda = 1.37$ is shown in Figure 1F, indicating significant hysteresis and six load drops of roughly equivalent magnitude. The force–displacement response is essentially unchanged after seven cycles, demonstrating full recoverability of this SRM. An estimation of the snap-through strength of the periodic material from analytical methods (discussed later in this article) is also shown in this figure. Figure 1G shows a 3D version of the proposed high-strength SRM.

The ability to capture the load–displacement response of multistable structures with analytical or numerical models is essential for design activities. Here, we show that such response can be obtained from the mechanical behavior of its constituent bi-stable triangular units shown in Figure 1A. The problem of a bi-stable triangular unit under vertical force can in turn be reduced to the response of an inclined guided beam restrained between two vertical walls,[20–22] due to the reflection symmetry of the unit about the vertical center line (dashed), and also the fact that the triangle base is relatively rigid and thus cannot bend or stretch. An analytical method was used in this study to obtain the load–displacement response of inclined guided beams with living hinges based on the beam-deflection method,[23] providing us with great insight on the underlying physics at different stages of response of the bi-stable element with non-convex elastic energy. The analytical method assumes that the overall deflection of the beam can be expressed as a superposition of three deflection modes, namely, axial stretching, symmetric bending, and asymmetric bending (see Section B, Supporting Information). Analysis shows that the load–displacement response of a uniform inclined guided beam follows five consecutive stages, as shown in **Figure 2**A. In the first stage the beam is subject to purely axial compression due to the stretching dominated static and kinematic response of the structure under small deformations,[24] and the behavior is almost linear. In general, this stage is abruptly ended at the normalized critical load of $4\pi^2 \sin\alpha$, where the structure suddenly buckles into the well-known problem of a column with two fixed ends under axial compression. During this second stage, the load–displacement response has a negative slope (spinodal phase) and the deformation is almost purely symmetric. In stage 3, the deformation is a combination of symmetric and asymmetric components and the slope is negative (continued spinodal phase). In stage 4, the symmetric component of deformation disappears, and the response takes a positive slope again. Finally in stage 5, the behavior becomes purely stretching dominated. If the thickness-to-length ratio of the hinges is sufficiently large, the symmetric buckling strength of the inclined beams is higher than the maximum axial load induced in the beams during snap-through, and no bifurcation in the load–displacement response is observed. In this case, the load–displacement response consists of only three stages and the slope changes continuously during the transitions from axial compression to asymmetric deformation and from asymmetric deformation to axial stretching (see Section C, Supporting Information).

As discussed above, the normalized snap-through strength of uniform inclined guided beams of various angles is bound by $4\pi^2$, which significantly limits the strength and energy absorption capacity of the triangular units and consequently the proposed structures. To amend this, we replace the inclined beam with uniform cross section in this design with a stepped beam consisting of a relatively thick and rigid section in the middle and two sections of equal length with smaller cross section on the two sides as shown in Figure 2B. The parameter R is defined as the ratio between the rigid section and the overall beam length as shown in the inset of Figure 2B. As R approaches 1, we are essentially creating a beam with two living hinges on each side, localizing the strain energy of the deformed structure at those regions. Figure 2B shows the force–displacement response of inclined beams with $\alpha = 15^\circ$ for different values of R, confirming that the snap-through strength and negative stiffness increase significantly by increasing R. On the other hand, the localization of deformation at hinges by increasing R can lead to their premature failure: for a given base material and hinge design (i.e., given combinations of α and R), a critical hinge thickness will exist above which the material would yield or fracture upon snap-through, thus preventing reconfigurability. This critical condition is discussed in detail below.

In Figure 2C, we plot the absorbed energy per unit volume (energy density) of the stack of unit cells shown in inset of Figure 2D until full densification (this energy is represented schematically by the hatched area in the figure inset) as a function of angle, α, and length ratio, R. The energy density is normalized by $E(t/L)^3$, where E, t, and L denote the material Young's modulus, hinge thickness, and overall inclined beam length, respectively (note that energy scales with $(t/L)^3$ when $t/L \ll 1$). The white region on the top right hand corner of the plot bordered by dashed line embodies combinations of R and α that are not kinematically feasible for a bi-stable mechanism, as the length of the rigid section is so large (i.e., $R > \sin(\alpha)$) that it cannot rotate clear of the two side walls. The aspect ratio of the hinges, t/L, plays a critical role on the structural integrity and mechanical performance of the proposed SRMs. Analytical calculations presented in section B of the Supporting Information allow derivation of close form expressions for the maximum strain developed in the hinges upon snap-through. To prevent failure, this strain must be lower than the yield or fracture

ADVANCED MATERIALS
www.advmat.de

www.MaterialsViews.com

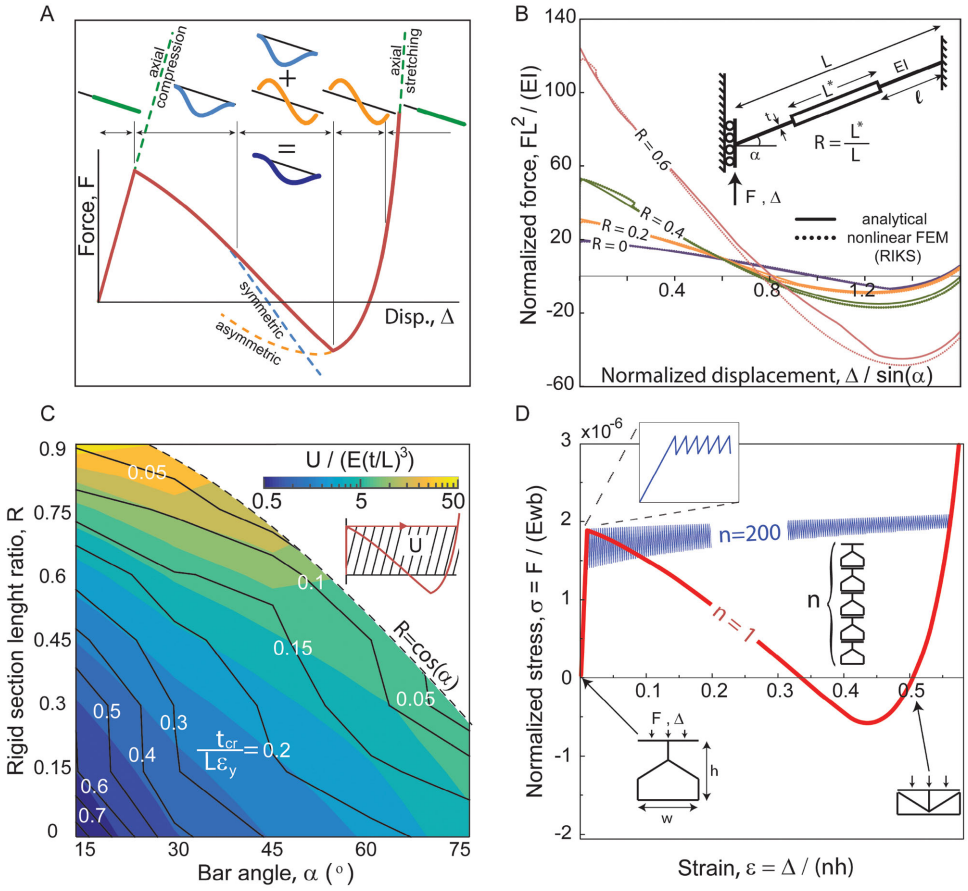

Figure 2. A) Schematic of the load–displacement response of a uniform inclined guided beam showing five distinct stages of deformation. B) The load–displacement response of an inclined guided beam with rigid middle section with length ratios of $R = 0$, 0.2, 0.4, and 0.6 from analytical and FE methods. C) Logarithmic-scale contour plot of absorbed energy per unit volume until full densification for the 1D shape-reconfigurable structure shown in (D) as a function of R and α. The energy is normalized by $E(t/L)^3$, where E is the Young's modulus of the base material. The overlaid contour lines show the maximum allowable hinge thickness to avoid hinge failure (by yielding or fracture), normalized by $L \cdot \varepsilon_y$. D) The normalized stress–strain response of a single bi-stable unit (red) and a stack of 200 bi-stable units (blue) under quasi-static displacement control compression obtained numerically.

strain of the hinge material. This condition can be cast as a limit on the maximum allowable aspect ratio of the hinges, normalized by the yield or fracture strain of the material, i.e., $t^{cr}/\varepsilon_y L$. Any thickness value greater than t^{cr} would cause the hinge to fail before snapping. Contours of this quantity are overlaid on Figure 2C. Our theoretical analysis shows that for linear elastic materials with relatively small values of elongation at failure ($\varepsilon_y < 0.1$), a category that includes most available materials, the value of critical hinge thickness ratio, t^{cr}/L, scales with ε_y, and the maximum strength and dissipated energy per unit volume of the SRM both scale with $E\varepsilon_y^3$ (see Section D, Supporting Information). However, for $\varepsilon_y \gg 1$ (representative of many elastomers), the critical hinge aspect ratio scales with $\varepsilon_y^{1/2}$, whereby the maximum strength and dissipated energy per unit volume both scale with $E\varepsilon_y^{3/2}$. In either case, the choice of the optimal material is dictated by a trade-off between maximizing the maximum allowable feature size ($\sim \varepsilon_y$ or $\varepsilon_y^{3/2}$), thus requiring less sophisticated manufacturing techniques, and maximizing the structural performance ($\sim E\varepsilon_y^3$ or $E\varepsilon_y^{3/2}$). The implication is that often stiffer and less deformable constituents (e.g., steel) might result in lower performance SRMs than softer constituents with larger strain to failure (see discussion of **Figure 3**B).

Contrary to continuum systems with convex elastic energy, the stress–strain response and the hysteresis behavior of a chain of discrete bi-stable elements differs significantly from that of a single element.[25] In order to study the behavior of a stack of bi-stable units, a numerical code is developed that allows calculation of macroscopic behavior of material based on a generic stress–strain behavior of a single element obtained from the numerical method, without requiring tri-linear or cubic approximations (see Section E, Supporting Information). Figure 2D compares the stress–strain response of a stack of 200 bi-stable units (blue) and a single unit (red) under quasi-static displacement control compression. Upon loading the stack, one or more of the bi-stable units that have the lowest strength values (e.g., due to material imperfections and geometrical variations) will snap-through (shrink) first at a stress value close to the nominal strength, causing the other cells in the stack to partially relax and the load to drop as shown by the blue curve in Figure 2D. This sequence of gradual increase and sudden drop in the stack reaction force continues until all the cells in the stack collapse and full densification is reached. The resulting hysteresis from different paths during loading and unloading due to cell relaxation at a fix displacement renders the energy absorption

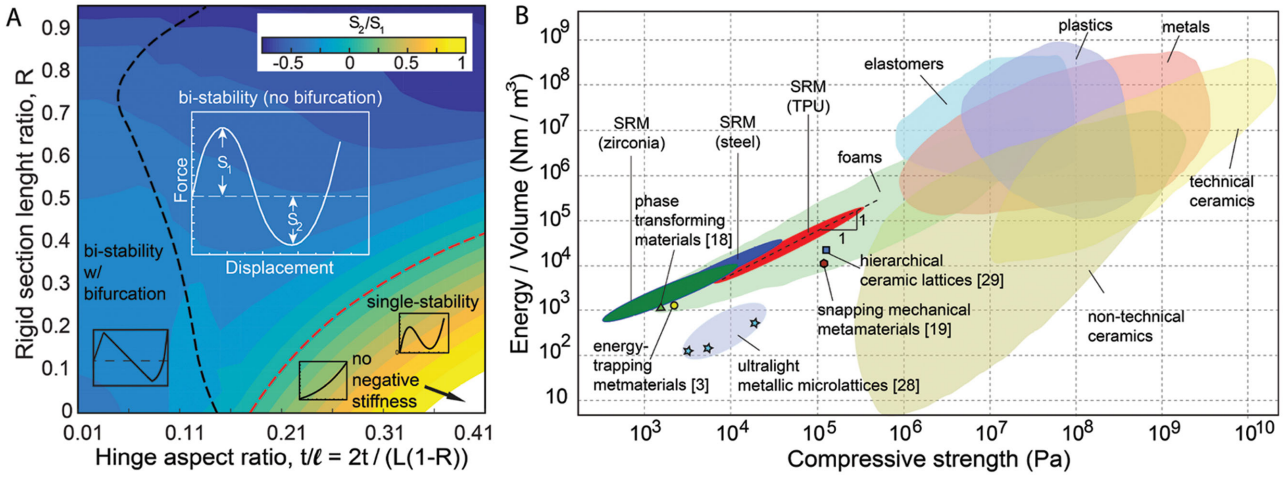

Figure 3. A) Phase stability parameter, S_2/S_1, for a structure with $a = 15^{\circ}$. B) Ashby plot of the absorbed energy per unit volume versus the compressive strength for the universe of existing materials and the proposed high-strength architected SRM.

capacity of the tessellated structure significantly higher than the sum of those of the individual units (i.e., the area under the red curve). The difference in absorbed energy is dissipated through mechanical vibrations of the collapsing and relaxing cells at each load drop. This strategy can also be used to obtain a significant range of deformation at a relatively constant load. In human and animal muscle fibers, thousands of multistable titin molecules linked in series are responsible for creating a relatively constant reaction force over a significant range of tissue stretch, which is essential for muscle's passive elasticity.[26]

For applications involving shape reconfigurability, the stability of the various deformed phases is critical. The phase stability in general is affected by the non-dimensional rigid section length R, the hinge angle α, and the hinge thickness ratio $t/\ell = t/L \cdot (2/(1-R))$, where ℓ is the hinge length. In Figure 3A, the phase stability parameter, defined as S_2/S_1, is plotted versus t/ℓ and R for a constant $a = 15^{\circ}$. Here, S_1 and S_2 denote the maximum and minimum force values between the first and third equilibrium points, respectively (see figure inset). The figure shows three distinct regions of stability behavior. The region on the left is when the hinge thickness ratio is small, therefore the values of S_1 and negative stiffness are controlled by the buckling induced symmetric bending of the beam in the negative stiffness (spinodal) phase. When hinge thickness is over 0.17 and R is small, the structure is single stable and $S_2 > 0$. The middle region represents cases where the structure is bi-stable, however the slope of the force–displacement curve is continuous due to a more significant contribution of axial stretching (e.g., $t/\ell > \sqrt{(9\alpha^3)/(4\pi^2 \sin(\alpha))}$ when $R = 0$, see Section C, Supporting Information). The slope of the curve at different phases is critical to the multi-cell behavior of multistable unit chains.[25] The results also show that the use of stepped beams (i.e., $R > 0$) significantly expands the bi-stable region.

For energy absorption applications, juxtaposition of the performance of the proposed materials with universe of existing materials is instructive. Figure 3B shows an Ashby map of absorbed energy per unit volume versus compressive strength. Materials in the top left corner of the map will be optimal from an impact resistance perspective.[27] Results for different base materials are presented: an elastomer (TPU), a metal (steel), and a ceramic (zirconia). The rationale for the choice of these materials is presented in Section D of Supporting Information. Although the metal and ceramic constituent materials have much higher values of strength, the elastomeric SRM has superior compressive strength compared to metal and ceramic SRMs. This is due to significantly lower values of yield (failure) strain, ε_y,for metals and ceramics, which results in extremely thin hinges in order to avoid hinge failure. The proposed shape-reconfigurable material overlays part of performance region of elastomers and outperforms previously proposed micro-lattices with substantial recoverability from large strains including ultralight and hierarchical architected materials.[28,29] Only the architected materials presented in this work, however, are multistable.

In summary, we propose a novel multistable shape-reconfigurable architected material based on a structural building block encompassing living hinges. 1D, 2D, and 3D architected materials can be designed, enabling complex shape morphing patterns. One of the key benefits of the proposed multistable designs for application such as shape reconfigurability and energy absorption is the reversibility between different stable states, implying that the original or deformed configurations of the material can be infinitely recovered with no compromise on the efficiency, integrity, or life of the structure. However, the localization of the majority of trapped strain energy on the hinges makes the failure strain of the hinge material critical to the viability of the proposed concepts and imposes significant restraints on material selection. This requirement is material-specific and is investigated comprehensively in this study. Reducing the feature size in these materials is shown to be a possible solution for creating hinges that will undergo snapping without plastic deformation. Both metals and ceramics generally become stronger as the critical length scale is reduced (by virtue of well-established size effects in plasticity and fracture), making the failure strain of the hinge material significantly higher at the nanoscale and thus resulting in more efficient multi stable designs.[30–32] Reducing the size of the unit cell could also lead to increased smoothness of the outlines in the desired topologies, thus enabling better dimensional control.

Finally, scale reduction in the unit cell generally results in a larger number of unit cells per unit volume in the macroscale structure, which enhances energy dissipation in discrete materials systems with negative stiffness mechanisms.[25,33] Future studies will address the manufacture of proposed material at the micro- and nanoscales.

Supporting Information

Supporting Information is available from the Wiley Online Library or from the author.

Acknowledgements

Funding from Office of Naval Research (Program Manager: D. Shifler, Contract No. N000141110884) is gratefully acknowledged. J.H. acknowledges partial support from the Air Force Office of Science Research under Award No. FA9550-15-1-0321 (Program Officer: Byung "Les" Lee). The Abaqus Finite Element Analysis software is licensed from Dassault Systemes SIMULIA, as part of a Strategic Academic Customer Program between UC Irvine and SIMULIA.

Received: March 25, 2016
Revised: May 27, 2016
Published online: July 6, 2016

[1] G. Tibert, *Deployable Tensegrity Structures for Space Applications* **2002**, Royal Institute of Technology, Stockholm, Sweden.
[2] A. Hanaor, R. Levy, *Int. J. Sp. Struct.* **2009**, *16*, 211.
[3] S. Shan, S. H. Kang, J. R. Raney, P. Wang, L. Fang, F. Candido, J. A. Lewis, K. Bertoldi, *Adv. Mater.* **2015**, *27*, 4296.
[4] S. Babaee, N. Viard, P. Wang, N. X. Fang, K. Bertoldi, *Adv. Mater.* **2015**, *28*, 1631.
[5] D. M. Correa, T. Klatt, S. Cortes, M. R. Haberman, D. Kovar, C. Seepersad, *Rapid Prototype J.* **2015**, *21*, 193.
[6] B. Haghpanah, H. Ebrahimi, D. Mousanezhad, J. Hopkins, A. Vaziri, *Adv. Eng. Mater.* **2015**, *18*, 643.
[7] Z. You, *Science* **2014**, *345*, 623.
[8] S. Felton, M. Tolley, E. Demaine, D. Rus, R. Wood, *Science* **2014**, *345*, 644.
[9] J. Henrickson, R. Skelton, J. Valasek, *AIAA Guidance, Navigation, and Control Conf.* **2016**, p. 1864.
[10] J. Henrickson, J. Valasek, R. Skelton, *AIAA Space 2015 Conf. & Exp.* **2015**, p. 4502.
[11] S. M. Felton, M. T. Tolley, B. Shin, C. D. Onal, E. D. Demaine, D. Rus, R. J. Wood, *Soft Matter* **2013**, *9*, 7688.
[12] D. Restrepo, N. Mankame, P. Zavattieri, *Proc. Exp. Mech.* **2011**, *3*, 105.
[13] S. Follmer, D. Leithinger, A. Olwal, N. Cheng, H. Ishii, *Proc. 25th Annu. ACM Symp. Intf. Soft. & Tech.* **2012**, p. 519.
[14] K. Gilpin, K. Kotay, D. Rus, I. Vasilescu, *Int. J. Rob. Res.* **2008**, *27*, 345.
[15] M. Yim, W. Shen, B. Salemi, *Rob. Autom. Mag. IEEE* **2007**, *14*, 43.
[16] C. Yu, K. Haller, *IEEE/RSJ Int. Conf. Intell. Rob. Syst.* **2008**, p. 3571.
[17] J. Prasad, A. R. Diaz, *J. Mech. Des.* **2006**, *128*, 1298.
[18] D. Restrepo, N. D. Mankame, P. D. Zavattieri, *Extreme Mech. Lett.* **2015**, *4*, 52.
[19] A. Rafsanjani, A. Akbarzadeh, D. Pasini, *Adv. Mater.* **2015**, *27*,5931.
[20] J. Zhao, J. Jia, X. He, H. Wang, *J. Appl. Mech.* **2008**, *75*, 041020.
[21] C. Kim, D. Ebenstein, *J. Mech. Rob.* **2012**, *4*, 1.
[22] G. L. Holst, G. H. Teichert, B. D. Jensen, *J. Mech. Des.* **2011**, *133*, 051002.
[23] S. Timoshenko, J. Gere, *Theory of Elastic Stability* **1961**, McGraw-Hill, New York, USA.
[24] J. Maxwell, *Philos. Mag.* **1864**, *XXVII*, 294.
[25] G. Puglisi, L. Truskinovsky, *J. Mech. Phys. Solids* **2000**, *48*, 1.
[26] L. C. Junqueira, J. Carneiro, *Junqueiras's Basic Histology* **2013**, McGraw-Hill, London, UK.
[27] A. G. Evans, M. Y. He, V. S. Deshpande, J. W. Hutchinson, A. J. Jacobsen, W. B. Carter, *Int. J. Impact Eng.* **2010**, *37*, 947.
[28] L. Salari-Sharif, T. A. Schaedler, L. Valdevit, *J. Mater. Res.* **2014**, *29*, 1755.
[29] L. R. Meza, A. J. Zelhofer, N. Clarke, A. J. Mateos, D. M. Kochmann, J. R. Greer, *Proc. Natl. Acad. Sci. USA* **2015**, *112*, 11502.
[30] J. R. Greer, J. T. M. De Hosson, *Prog. Mater. Sci.* **2011**, *56*, 654.
[31] H. Gao, B. Ji, I. L. Jäger, E. Arzt, P. Fratzl, I. L. Jager, E. Arzt, P. Fratzl, I. L. Jäger, E. Arzt, P. Fratzl, *Proc. Natl. Acad. Sci. USA* **2003**, *100*, 5597.
[32] L. R. Meza, S. Das, J. R. Greer, *Science* **2014**, *345*, 1322.
[33] I. Benichou, S. Givli, *J. Mech. Phys. Solids* **2013**, *61*, 94.